International Journal of Thermophysics, Vol. 13, No. 3, 1992

High-Pressure Viscosity and Density of *n*-Alkanes

E. Kiran[1] and Y. L. Sen[1]

Received June 25, 1991

High-pressure viscosities and densities of *n*-butane, *n*-pentane, *n*-hexane, and *n*-octane have been measured with a specially designed falling cylinder viscometer. Data cover the pressure range from 10 to 70 MPa at temperatures from 310 to 450 K. When the viscosity is plotted as a function of density, the data at all temperatures and pressures are shown to reduce to a single curve for each alkane. An exponential relationship of the form $\eta = B_1 \times \exp(B_2 \times \rho) + B_3$ is used to describe the density dependence of viscosity. The logarithmic viscosity of the alkanes changes linearly with the inverse temperature at all pressures. The density shows a linear dependence on temperature.

KEY WORDS: butane; density; hexane; high pressure; octane; pentane; viscometer; viscosity.

1. INTRODUCTION

The viscosity and density of *n*-alkanes have already received considerable attention in the literature [1–25]. Publications by Stephan and Lucas [1] and by Liley et al. [2] review the viscosity of several fluids including *n*-butane, *n*-pentane, *n*-hexane, and *n*-octane and give recommended values in graphical and tabular forms. The recommended viscosity values are derived from the original data sources using some interpolation or extrapolation techniques. Other prevalent literature [3–13, 17–21, 23–25] dealing with the viscosity of these alkanes are summarized in Table I.

As can be seen from Table I, a wide range of experimental conditions has been covered. Temperatures vary from room temperature to as high as 569 K. Pressures vary from atmospheric pressure to as high as 1177 MPa. The methods used for the viscosity measurements include the capillary tube, falling cylinder, rolling ball, torsionally vibrating crystal, oscillating

[1] Department of Chemical Engineering, University of Maine, Orono, Maine 04469, U.S.A.

0195-928X/92/0500-0411$06.50/0 411 1992 Plenum Publishing Corporation

cup, and rotating cylinder techniques. It is, however, noted that viscosity data at high-pressure ranges are limited to relatively low temperatures, less than 373 K.

There is, however, an increasing need for viscosity data at high pressures and temperatures, especially at near- and supercritical conditions. This stems from the rapidly growing potential for the utilization of supercritical fluids as process solvents.

Table I. Literature on the Viscosity of *n*-Butane, *n*-Pentane, *n*-Hexane, and *n*-Octane

Fluid	Method of measurement	Temperature range (K)	Pressure range (MPa)	Reference
n-Butane	Capillary tube	311–444	0.1–55	Dolan et al. [23]
	Rolling ball	303	0.1–1000	Babb & Scott [17]
	Torsionally vibrating crystal	115–300	0.1–30	Diller & Van Poolen [25]
	Rotating cylinder	277–433	0.1–34.5	Carmichael & Sage [24]
n-Pentane	Capillary tube	311–444	1.4–20.7	Lee & Ellington [19]
	Capillary tube	298–548	0.1–51	Agaev and Golubev [20]
	Falling cylinder	303–348	0.1–1177	Bridgeman [6]
	Rolling ball	273–333	0.1–400	Brazier & Freeman [4]
	Rolling ball	303	0.1–1000	Babb & Scott [17]
	Torsionally vibrating crystal	303–323	0.1–686	Collings & McLaughlin [21]
	Rotating cylinder	311–411	0.7–35	Reamer et al. [18]
n-Hexane	Capillary tube	283–378	Saturated liquid	Dymond & Young [7]
	Capillary tube	288–548	0.1–50.7	Agaev & Golubev [10]
	Capillary tube	297–333	0.1–39.2	Naziev et al. [11]
	Falling cylinder	298–373	0.1–500	Dymond et al. [12]
	Falling cylinder	303–348	0.1–1177	Bridgeman [6]
	Falling cylinder	303	0.1–500	Dickinson [9]
	Rolling ball	273–333	0.1–400	Brazier & Freeman [4]
	Torsionally vibrating crystal	298–348	0.1–110	Kashiwagi & Makita [3]
	Oscillating cup	293–423	1–40	Berstad [13]
n-Octane	Capillary tube	323–569	0.1–50.7	Agaev & Golubev [5]
	Capillary tube	283–378	Saturated liquid	Dymond & Young [7]
	Falling cylinder	303–348	0.1–1177	Bridgeman [6]
	Falling cylinder	303	0.1–500	Dickinson [9]
	Falling cylinder	298–373	0.1–500	Dymond et al. [8]
	Rolling ball	273–333	0.1–400	Brazier & Freeman [4]
	Torsionally vibrating crystal	298–348	0.1–110	Kashiwagi & Makita [3]

In this paper, we report high-pressure viscosity and density data for *n*-butane, *n*-pentane, *n*-hexane, and *n*-octane over a wide pressure and temperature range. A pressure range from about 10 to 70 MPa at temperatures from about 310 to 450 K has been covered. The data were obtained with a newly designed falling cylinder viscometer which is equipped with a variable-volume view cell and permits the determination of both the viscosity and the density.

2. EXPERIMENTAL

2.1. Viscometer System

A schematic diagram of the experimental system is shown in Fig. 1 [26]. Briefly, the system consists of a view cell (VC) equipped with a fall tube (FT) attachment, and a variable-volume part (VVP), which are all enclosed in an air-heated oven. The viscosity measurements are based on the measurement of the fall time of a cylindrical sinker using three LVDT coils (C1). Density measurements are based on the measurement of the viscometer volume at any time during an experiment by monitoring the movement of a piston with the help of a designated LVDT coil (C2). The

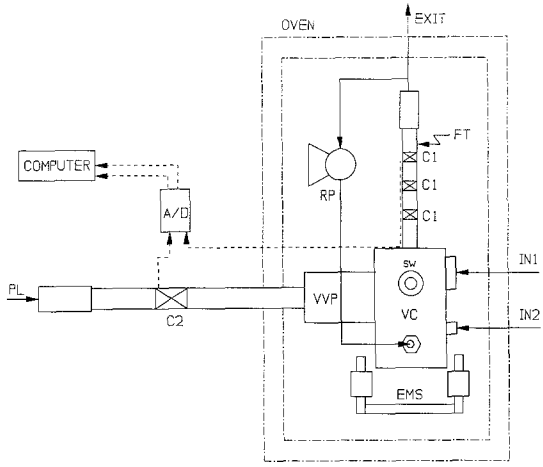

Fig. 1. A schematic diagram of the viscometer system. VC, View cell; VVP, variable-volume part; FT, fall tube attachment; RP, recirculation pump; C1, linear variable differential transformer (LVDT) coils; C2, LVDT coil for piston position; EMS, electromagnetic stirrer; SW, sapphire windows; IN1 and IN2, sample ports 1 and 2; PL, pressure line; A/D, signal conditioning units and analog-to-digital converter.

viscometer has two sapphire windows (SW) which permit visual inspection of the fluid under examination. When needed, the cell content is mixed with the aid of either an external electromagnetic stirrer (EMS), a recirculation pump (RP), or both.

The viscometer tube (20.32 cm long, 0.794-cm ID, 1.429-cm OD) is made of nonferromagnetic 316 stainless steel. The total length available for the fall of the sinker in the tube is 15 cm. The sinker is 0.7685 cm in diameter, 2.0915 cm in length and made of ferromagnetic 416 stainless steel and thus magnetically permeable. The leading end of the sinker is machine to be hemispherical. The edges of the trailing end are slightly machined to improve stability. The ratio of sinker-to-tube radii (r_1/r_2) is 0.9682, which is greater than the 0.93 needed to ensure concentric fall [27–29] and error-free fall-time measurements.

A stepper motor is used to move an electromagnetic pull-up magnet up or down the fall tube, along the outside periphery of the LVDT coils. This magnet is used primarily to bring the sinker to the top position in the fall tube before each fall-time measurement is initiated.

The viscometer temperature is measured with an accuracy of ± 1.5 K using a J-type thermocouple and read with a resolution of 0.1 K. Pressures are measured with an accuracy of ± 0.06 MPa using a Dynisco transducer and read with a resolution of 0.007 MPa. Pressure readings are calibrated using a Heise gage. The fall-time data are recorded with a computer with an accuracy of ± 2 ms. Volume displacements are determined with $\pm 0.2\%$ accuracy.

Following the fluid charge, the system is heated up and the conditions are adjusted to the experimental temperature and pressure. At a given temperature, pressure manipulations are carried out by changing the position of the piston in the variable-volume part of the cell by applying pressure from the pressure line (PL). Once the thermal equilibrium is reached, the temperature, pressure, and piston position are all recorded whenever a fall-time measurement is taken. During fall-time measurements, the recirculation pump is stopped. At a given temperature, viscosity determinations are carried out at different pressures up to 70 MPa. At each temperature and pressure, several consecutive fall-time measurements are taken. Sufficient time is allowed between consecutive repeat measurements to ensure equilibration. Other system and operational details have been described elsewhere [30, 31].

2.2. Calibration

The viscometer was calibrated with fluids of known viscosity and density. A two-step procedure has been followed. In the first step, calibra-

tion was carried out at atmospheric pressure and low temperatures using the NBS certified viscosity standards N.4, N.8, N1.0, S6, and S20 obtained from Cannon Instrument Co., State College, PA. Fall times were measured at 313 K for N.4, N.8, and N1.0 and at 313 and 373 K for S6 and S20. In the second step, the instrument was calibrated for high pressures and temperatures using *n*-hexane and viscosity data from the literature. This step involves determination of a temperature- and pressure-dependent correction factor for calibrations. Literature data for *n*-hexane viscosity were taken from Naziev et al. [11], who report data at 313 K up to 39.2 MPa, and from Agaev and Golubev [10], who report data at 323, 348, 373, 398, 423, and 488 K up to 50 MPa. Densities for *n*-hexane were experimentally determined in the present study at each temperature and pressure.

In the first step of the calibration procedure, several consecutive fall-time measurements (about 10 or more) are taken for a given standard. The fall times corresponding to three fall distances, i.e., between each pair of coils are then averaged. The average fall times are related to the viscosity (η) and density (ρ) of the standards using

$$\eta = \{K(t)[\rho_s - \rho] \tag{1}$$

where $K(t)$ is a fall time-dependent calibration parameter and ρ_s is the density of the sinker. The fall-time dependence of K is obtained by using the known viscosity and density of the standards and plotting $\eta/(\rho_s - \rho)$ as a function of all time t corresponding to each distance between any pair of the three coils. Under ideal laminar flow conditions, the dependence is of the form,

$$K = kt \tag{2}$$

Table II. Low-Pressure/Low-Temperature Calibration Data[a]

Viscosity standard	Calibration temp. (°C)	η (mPa·s)	ρ (g·cm^{-3})	Average fall times (s), coils 1–2	Calibration parameter K $[\eta/(\rho_s - \rho)]$
N.4	39.4	0.2699	0.6522	1.156	0.03776
N.8	39.4	0.5246	0.8499	1.868	0.0755
N1.0	39.1	0.8168	0.7816	2.593	0.1164
S6	99.7	1.4496	0.8052	4.169	0.2072
S20	99.5	3.0940	0.8080	8.713	0.4425
S6	39.3	4.9010	0.8457	14.866	0.7047
S20	38.9	16.2590	0.8466	48.910	2.3383

[a] η and ρ are the viscosity and density of the standard at the calibration temperature as given by the supplier and ρ_s is the sinker density (7.8 g·cm^{-3} [32]).

where the proportionality constant k is the ideal instrument constant which depends only on the geometry of the instrument.

Table II shows the average fall times between the first two coils for the various viscosity standards at the indicated temperatures. The average fall times for the other coil pair were similar. Figure 2 shows the dependence of instrument calibration parameter K on fall time. This dependence is described by two linear equations, which are applicable for fall times greater and less than 5 s.

$$K = 1.25858 \times 10^{-2} + 4.7555144 \times 10^{-2} t \quad \text{for} \quad t \geqslant 5 \text{ s} \tag{3}$$

$$K = -2.88637 \times 10^{-2} + 5.64393 \times 10^{-2} t \quad \text{for} \quad t < 5 \text{ s} \tag{4}$$

The 5-s fall time corresponds to viscosities around 3 mPa · s. The literature indicates that the flow of fluid around the sinker may start to show deviations from laminar conditions at viscosities below about 4 mP · s [8]. At higher viscosities, laminar flow conditions are assured and the instrument calibration parameter should be describable by Eq. (2) and should pass through the origin. However, to account for any deviations from laminar flow conditions, the calibration Eqs. (3) and (4) have not been forced to pass through the origin.

For viscosity determinations at high temperatures and pressures, K, which so far has been considered to be only a function of fall time, has to

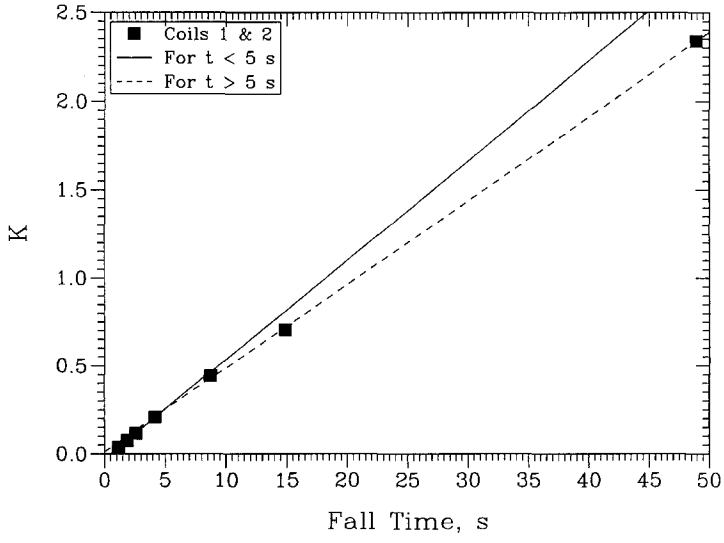

Fig. 2. Dependence of the instrument calibration parameter K on fall time.

be modified to consider its dependence on temperature and pressure. This is achieved by incorporating a temperature- and pressure-dependent correction factor $X(T, P)$. The relationship for viscosity then becomes

$$\eta = \{K(t)/X(T, P)\}[\rho_s - \rho] \tag{5}$$

This correction factor was determined by performing a series of fall-time measurements as a function of pressure at different temperatures using *n*-hexane as a standard. The fall times were measured at pressures from about 7 to 70 MPa and temperatures of 313, 323, 348, 373, 398, 423, and 448 K. They were then converted to viscosity values using Eqs. (3) and (4). The viscosity values thus estimated were compared with the literature values. The ratio of the estimated viscosities to the literature values, η_{est}/η_{lit}, were plotted as a function of pressure (expressed in units of MPa) at several different temperatures. First-order polynomials of the form

$$\eta_{est}/\eta_{lit} = a + bP \tag{6}$$

were fitted to the data at each temperature. The coefficients a and b were determined for each coil distance at the calibration temperatures.

Then the viscosity ratios, η_{est}/η_{lit}, were calculated at constant pressures of 0.1, 1, 3, 5, 8, 10, 13, 15, 18, 20, 25, 30, 35, 40, 45, 55, 55, 60, 65, and 70 MPa at each of the above temperatures using the coefficients of the first-order polynomials obtained with Eq. (6). This time, the viscosity ratios were plotted as a function of temperature at constant pressures. At each pressure, second-order polynomials were fitted to the data for each coil distance, i.e.,

$$\eta_{est}/\eta_{lit} = A + BT + CT^2 \tag{7}$$

where T is in °C. The viscosity ratio, η_{est}/η_{lit}, obtained from Eq. (7) already incorporates pressure dependence and is used as the temperature/pressure-dependent correction factor $X(T, P)$.

The high-pressure and temperature calibration procedure that has just been described covers all the effects of temperature and pressure on the fall times due to the changes in the dimensions of the fall tube and the sinker.

Following these procedures, viscosities and densities are determined with an accuracy of ± 3 and ± 1 % or better, respectively. This is illustrated in Figs. 3 and 4 for *n*-pentane. Viscosity and density data obtained with the present system are compared with those from the literature [19, 20, 22] at different temperatures. For data sets at identical temperatures, the values are in very close agreement and within these accuracy limits. For data at slightly different temperatures, there are differences, and the differences are

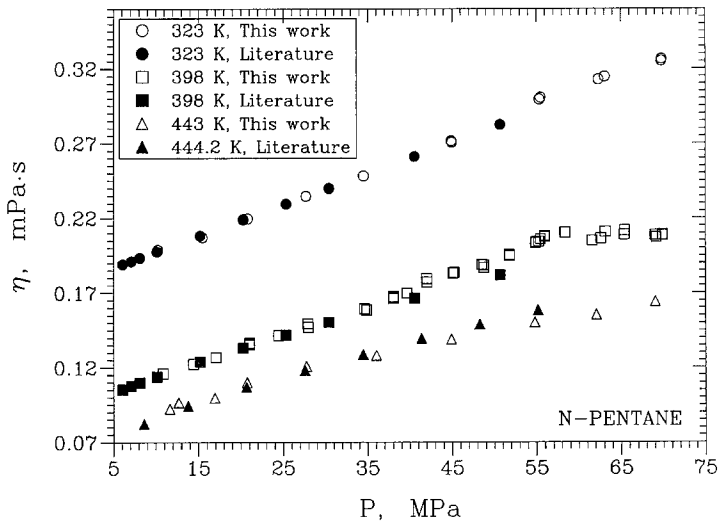

Fig. 3. Comparison of the viscosity of *n*-pentane with the literature. (Literature data at 323 and 398 K are from Ref. 20, and those at 444.2 K from Ref. 19.)

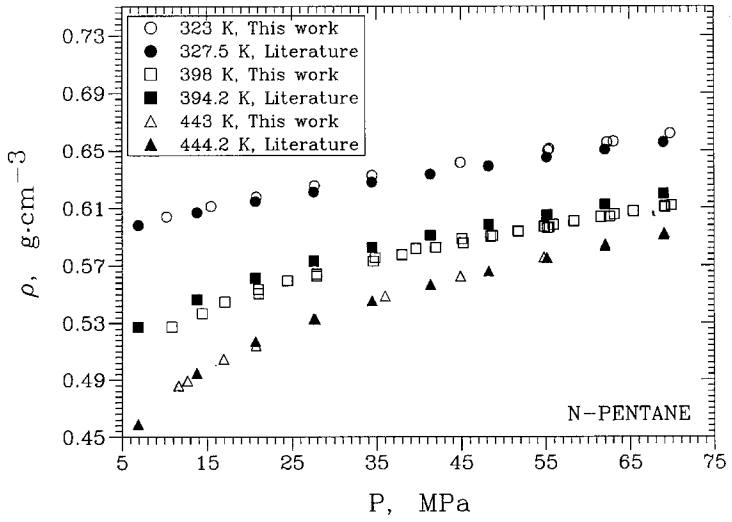

Fig. 4. Comparison of the density of *n*-pentane with the literature. (Literature data from Ref. 22.)

Table III. The Normal Boiling Points and the Critical Properties of *n*-Butane, *n*-Pentane, *n*-Hexane, and *n*-Octane [33]

n-Alkane	T_b (K)	T_c (K)	P_c (MPa)	ρ_c (g·cm^{-3})
Butane	272.7	425.2	3.80	0.2279
Pentane	309.2	469.7	3.37	0.2373
Hexane	341.9	507.5	3.01	0.2329
Octane	398.8	568.8	2.49	0.2322

in accordance with the direction of change in the temperature. The reliability of the system has been further checked and verified with other fluids such as *n*-butane, *n*-hexane, and *n*-octane.

2.3. Materials

The alkanes were obtained from Matheson (*n*-butane; purity, 99.9%) and from Aldrich Chemical Co. (*n*-pentane, *n*-hexane, and *n*-octane; purity, >99%) and used without further purification. The physical properties of these *n*-alkanes are given in Table III.

3. RESULTS AND DISCUSSION

3.1. General Observations

The numerical values of the viscosities and densities for *n*-butane, *n*-pentane, *n*-hexane, and *n*-octane are tabulated in Tables IV, V, VI, and VII, respectively. Both viscosity and density increase with the carbon number of the alkane. For each alkane, viscosity and density increase with pressure but decrease with temperature. This is illustrated in Figs. 3 and 4 for *n*-pentane.

3.2. Effect of Density

Figures 5, 6, 7, and 8 show the variation of viscosity with density. In these figures, all data points given in Table IV–VII have been included. For each alkane, density proves to be a good scaling parameter; reducing the data at all temperatures to a single curve.

The variation of viscosity with density is described well with an exponential equation of the form

$$\eta = B_1 \exp(B_2 \rho) + B_3 \tag{8}$$

Table IV. Experimental Density and Viscosity Data of *n*-Butane

P (MPa)	ρ (g · cm^{-3})	η (mPa · s)
	$T = 323$ K	
13.31	0.5674	0.1497
18.03	0.5759	0.1601
21.98	0.5819	0.1694
26.85	0.5888	0.1775
29.76	0.5927	0.1857
31.92	0.5951	0.1935
34.25	0.5974	0.1962
34.54	0.5984	0.1988
34.56	0.5984	0.1967
37.21	0.6014	0.1932
43.59	0.6077	0.1961
52.27	0.6162	0.2118
61.42	0.6244	0.2281
68.37	0.6295	0.2386
68.39	0.6295	0.2390
	$T = 348$ K	
13.86	0.5419	0.1212
21.19	0.5564	0.1378
28.11	0.5674	0.1454
34.75	0.5767	0.1572
34.77	0.5767	0.1576
41.35	0.5852	0.1746
44.67	0.5891	0.1770
48.37	0.5933	0.1879
48.39	0.5933	0.1850
51.81	0.5971	0.1978
55.09	0.6005	0.2050
55.10	0.6005	0.2052
58.53	0.6039	0.1942
62.02	0.6074	0.2005
62.06	0.6078	0.2020
65.59	0.6111	0.2036
68.50	0.6143	0.2056
69.17	0.6145	0.2072

Table IV. (*Continued*)

P (MPa)	ρ (g·cm^{-3})	η (mPa·s)
	$T = 373$ K	
15.17	0.5178	0.1063
17.16	0.5228	0.1108
21.12	0.5321	0.1169
21.21	0.5321	0.1174
27.58	0.5443	0.1256
27.63	0.5443	0.1257
34.38	0.5557	0.1342
34.58	0.5557	0.1332
41.46	0.5658	0.1462
48.34	0.5743	0.1543
48.38	0.5743	0.1557
55.16	0.5825	0.1698
58.51	0.5864	0.1722
62.08	0.5898	0.1780
63.75	0.5917	0.1817
66.94	0.5949	0.1883
69.12	0.5972	0.1935
	$T = 398$ K	
17.54	0.4959	0.0971
18.39	0.4988	0.0998
22.21	0.5100	0.1048
22.26	0.5096	0.1038
27.62	0.5222	0.1098
34.45	0.5339	0.1181
34.46	0.5339	0.1187
41.37	0.5456	0.1268
45.54	0.5490	0.1326
48.14	0.5554	0.1365
58.63	0.5670	0.1483
62.22	0.5718	0.1532
65.19	0.5744	0.1592
68.89	0.5786	0.1631
68.92	0.5781	0.1628

Table IV. (*Continued*)

P (MPa)	ρ (g · cm^{-3})	η (mPa · s)
	$T = 413$ K	
14.19	0.4675	0.0805
16.93	0.4781	0.0883
21.67	0.4938	0.0930
27.62	0.5094	0.1023
34.46	0.5229	0.1097
41.55	0.5350	0.1184
48.43	0.5459	0.1251
55.13	0.5556	0.1346
55.15	0.5556	0.1349
62.33	0.5646	0.1405
69.00	0.5717	0.1495
69.01	0.5717	0.1499
	$T = 428$ K	
21.28	0.4783	0.0782
27.32	0.4951	0.0912
32.31	0.5081	0.1005
37.94	0.5192	0.1049
43.33	0.5275	0.1093
48.57	0.5356	0.1156
53.78	0.5436	0.1193
58.60	0.5492	0.1253
63.82	0.5564	0.1314
69.14	0.5624	0.1398
	$T = 443$ K	
20.77	0.4621	0.0729
20.82	0.4621	0.0729
27.70	0.4842	0.0882
27.71	0.4835	0.0880
34.64	0.5019	0.0941
41.27	0.5141	0.1023
48.23	0.5266	0.1098
48.26	0.5266	0.1088
55.05	0.5366	0.1122
61.91	0.5450	0.1180
62.10	0.5465	0.1173
68.96	0.5540	0.1230
69.06	0.5540	0.1224

Table V. Experimental Density and Viscosity Data of *n*-Pentane

P (MPa)	ρ (g · cm^{-3})	η (mPa · s)
	$T = 318$ K	
7.50	0.6066	0.1956
7.51	0.6066	0.1963
14.28	0.6154	0.2116
14.28	0.6155	0.2117
20.92	0.6220	0.2284
27.63	0.6294	0.2413
27.71	0.6292	0.2418
34.53	0.6366	0.2558
34.61	0.6366	0.2559
44.88	0.6459	0.2801
55.33	0.6544	0.3058
55.37	0.6544	0.3050
65.55	0.6623	0.3270
69.25	0.6649	0.3322
	$T = 323$ K	
10.22	0.6041	0.1988
15.46	0.6113	0.2072
20.78	0.6178	0.2197
27.68	0.6257	0.2348
34.50	0.6328	0.2483
44.90	0.6417	0.2717
44.94	0.6417	0.2706
55.31	0.6504	0.2994
55.33	0.6504	0.2993
62.30	0.6558	0.3127
63.05	0.6564	0.3146
69.74	0.6620	0.3251
69.76	0.6620	0.3264
	$T = 348$ K	
10.51	0.5795	0.1659
10.56	0.5795	0.1655
10.64	0.5795	0.1664
10.88	0.5797	0.1667
12.81	0.5831	0.1704
12.83	0.5831	0.1689
15.56	0.5870	0.1783
15.68	0.5868	0.1797
15.91	0.5875	0.1804
16.54	0.5885	0.1801
16.56	0.5885	0.1795

Table V. (*Continued*)

P (MPa)	ρ (g · cm^{-3})	η (mPa · s)
	$T = 348$ K	
20.79	0.5946	0.1971
20.81	0.5944	0.1977
20.83	0.5945	0.1991
20.87	0.5944	0.1972
21.01	0.5944	0.1977
27.83	0.6038	0.1987
28.38	0.6041	0.2012
28.47	0.6041	0.1987
34.95	0.6121	0.2085
36.48	0.6135	0.2147
45.10	0.6229	0.2333
45.81	0.6232	0.2345
55.18	0.6320	0.2578
55.49	0.6327	0.2557
62.94	0.6387	0.2670
63.17	0.6395	0.2698
69.45	0.6440	0.2788
69.88	0.6451	0.2808
70.26	0.6445	0.2822
	$T = 373$ K	
12.26	0.5574	0.1392
15.84	0.5645	0.1479
20.85	0.5730	0.1596
20.87	0.5727	0.1590
28.24	0.5836	0.1727
28.25	0.5838	0.1759
36.43	0.5953	0.1955
36.48	0.5953	0.1932
38.09	0.5973	0.1999
45.63	0.6055	0.2032
46.39	0.6063	0.2027
55.20	0.6146	0.2180
63.28	0.6222	0.2312
63.32	0.6222	0.2305
69.98	0.6280	0.2406

Table V. (*Continued*)

P (MPa)	ρ (g · cm^{-3})	η (mPa · s)
	$T = 398$ K	
10.85	0.5274	0.1160
14.42	0.5367	0.1224
17.08	0.5447	0.1269
21.04	0.5534	0.1364
21.05	0.5506	0.1354
21.06	0.5506	0.1359
24.47	0.5595	0.1416
27.91	0.5641	0.1495
29.97	0.5626	0.1470
34.62	0.5731	0.1595
34.86	0.5754	0.1586
38.01	0.5776	0.1664
39.03	0.5773	0.1674
39.65	0.4819	0.1698
41.98	0.5826	0.1795
42.01	0.5826	0.1772
45.08	0.5886	0.1832
45.24	0.5857	0.1835
48.48	0.5904	0.1889
48.71	0.5908	0.1886
48.74	0.5908	0.1870
51.77	0.5942	0.1957
51.79	0.5936	0.1948
54.84	0.5972	0.2035
54.91	0.5969	0.2039
55.25	0.5963	0.2044
55.44	0.5966	0.2059
55.93	0.5984	0.2081
55.94	0.5984	0.2076
58.36	0.6010	0.2103
61.57	0.6039	0.2050
62.59	0.6040	0.2064
63.13	0.6057	0.2109
65.37	0.6078	0.2090
65.41	0.6078	0.2117
69.03	0.6112	0.2087
69.14	0.6105	0.2072
69.88	0.6119	0.2090
69.90	0.6119	0.2086

Table V. (*Continued*)

P (MPa)	ρ (g · cm^{-3})	η (mPa · s)
	$T = 413$ K	
11.12	0.5125	0.1080
14.14	0.5204	0.1150
20.50	0.5356	0.1255
27.66	0.5506	0.1366
35.90	0.5637	0.1513
44.86	0.5767	0.1646
54.54	0.5878	0.1778
61.86	0.5954	0.1938
68.58	0.5954	0.2089
68.59	0.6023	0.2093
	$T = 428$ K	
14.24	0.5065	0.1054
20.66	0.5236	0.1192
27.60	0.5387	0.1284
35.77	0.5535	0.1388
44.83	0.5664	0.1540
54.11	0.5782	0.1615
61.11	0.5864	0.1758
68.44	0.5936	0.1843
	$T = 443$ K	
11.65	0.4858	0.0924
12.69	0.4893	0.0967
16.94	0.5046	0.0997
20.74	0.5142	0.1101
27.77	0.5325	0.1208
36.02	0.5487	0.1182
44.91	0.5625	0.1390
54.79	0.5757	0.1503
62.07	0.5848	0.1554
69.02	0.5927	0.1640

where η is in mPa · s and ρ in g · cm^{-3}. These are shown by the solid curves in the figures. The values of the adjustable parameters B_1, B_2, and B_3 in Eq. (8) are given in Table VIII for each alkane. These coefficients are valid for *n*-butane, *n*-pentane, and *n*-octane in the density ranges of 0.47–0.64, 0.48–0.67, 0.53–0.70, and 0.57–0.73 g · cm^{-3}, respectively. These density ranges correspond to a temperature range from about 310 to 450 K and a pressure range from about 10 to 70 MPa for these alkanes.

Table VI. Experimental Density and Viscosity Data of *n*-Hexane

P (MPa)	ρ (g · cm^{-3})	η (mPa · s)
	$T = 313$ K	
0.21	0.6416	0.2578
0.21	0.6416	0.2581
5.86	0.6486	0.2764
5.88	0.6486	0.2770
14.31	0.6577	0.3000
14.32	0.6577	0.3004
23.91	0.6674	0.3263
23.95	0.6674	0.3264
34.29	0.6768	0.3569
34.29	0.6768	0.3573
44.63	0.6852	0.3874
44.63	0.6852	0.3868
54.99	0.6933	0.4183
	$T = 323$ K	
6.70	0.6415	0.2538
6.83	0.6415	0.2538
15.13	0.6490	0.2798
15.13	0.6490	0.2776
23.99	0.6588	0.2997
24.01	0.6588	0.2995
34.33	0.6688	0.3281
34.39	0.6688	0.3280
44.64	0.6779	0.3576
44.66	0.6779	0.3576
54.99	0.6860	0.3887
55.00	0.6860	0.3900
63.92	0.6926	0.4191
	$T = 348$ K	
7.26	0.6188	0.2062
7.29	0.6188	0.2053
16.02	0.6258	0.2292
16.05	0.6258	0.2275
24.19	0.6362	0.2532
34.21	0.6476	0.2730
34.29	0.6476	0.2729
44.82	0.6578	0.2994
55.34	0.6671	0.3338
55.43	0.6671	0.3347

Table VI. (*Continued*)

P (MPa)	ρ (g · cm^{-3})	η (mPa · s)
	$T = 373$ K	
7.26	0.5936	0.1812
7.43	0.5943	0.1785
15.52	0.6064	0.2086
15.65	0.6053	0.2092
25.44	0.6202	0.2094
25.51	0.6198	0.2133
34.89	0.6306	0.2324
34.93	0.6308	0.2321
44.84	0.6434	0.2551
55.44	0.6510	0.2855
55.49	0.6510	0.2847
65.85	0.6593	0.3086
	$T = 398$ K	
7.74	0.5742	0.1421
15.08	0.5880	0.1666
24.73	0.6031	0.1928
34.24	0.6160	0.2058
44.54	0.6282	0.2222
54.96	0.6387	0.2401
65.34	0.6475	0.2671
	$T = 423$ K	
10.79	0.5534	0.1316
16.93	0.5645	0.1460
24.01	0.5570	0.1607
24.03	0.5781	0.1618
34.21	0.5926	0.1828
44.61	0.6071	0.2100
44.63	0.6068	0.2103
44.65	0.6067	0.2106
55.64	0.6199	0.2126
55.73	0.6196	0.2105
63.25	0.6270	0.2205
	$T = 448$ K	
13.16	0.5341	0.1140
20.58	0.5486	0.1299
27.44	0.5627	0.1507
27.48	0.5622	0.1514
34.26	0.5745	0.1584
34.30	0.5736	0.1586
41.10	0.5848	0.1693
41.16	0.5848	0.1696
52.30	0.6002	0.1880
52.49	0.5994	0.1885

Table VII. Experimental Density and Viscosity Data of *n*-Octane

P (MPa)	ρ (g · cm^{-3})	η (mPa · s)
	$T = 323$ K	
12.86	0.6847	0.4435
24.40	0.6955	0.4994
34.52	0.7040	0.5491
44.99	0.7119	0.6047
55.57	0.7193	0.6752
64.65	0.7253	0.7174
	$T = 348$ K	
8.73	0.6584	0.3353
15.49	0.6664	0.3637
24.05	0.6748	0.3907
34.91	0.6853	0.4344
44.80	0.6938	0.4784
55.65	0.7021	0.5368
65.30	0.7090	0.5858
	$T = 373$ K	
8.00	0.6394	0.2720
9.04	0.6407	0.2742
15.58	0.6468	0.3000
23.82	0.6560	0.3245
35.24	0.6675	0.3675
45.01	0.6764	0.4047
55.20	0.6853	0.4424
66.48	0.6939	0.4865
	$T = 398$ K	
13.57	0.6229	0.2451
22.50	0.6366	0.2726
23.87	0.6372	0.2794
34.57	0.6499	0.3043
41.85	0.6576	0.3286
44.90	0.6591	0.3353
55.44	0.6697	0.3694
58.45	0.6714	0.3762
65.68	0.6777	0.4009

Table VII. (*Continued*)

P (MPa)	ρ (g·cm^{-3})	η (mPa·s)
	$T = 423$ K	
14.85	0.6027	0.2160
23.50	0.6172	0.2398
33.24	0.6310	0.2607
36.64	0.6342	0.2654
46.64	0.6451	0.2930
56.40	0.6542	0.3143
63.39	0.6600	0.3340
66.35	0.6631	0.3360
	$T = 448$ K	
11.54	0.5796	0.1868
19.41	0.5914	0.2136
29.16	0.6082	0.2228
34.37	0.6146	0.2365
37.76	0.6184	0.2354
42.76	0.6248	0.2440
51.40	0.6339	0.2576
55.41	0.6388	0.2669
58.21	0.6427	0.2697

In Figs. 5, 6, and 7, a small local maximum in the viscosity of the corresponding alkane (especially visible in *n*-pentane) is observed in a density range from 0.60 to 0.61 g·cm^{-3}, which, when normalized with respect to the critical density of each alkane, corresponds to a ρ/ρ_c value in the range from 2.5 to 2.6. In these plots, viscosities at these local maxima have

Table VIII. Coefficients of the Exponential Equation $\eta = B_1 \exp(B_2\rho) + B_3$ for the Density Dependence of Viscosity of *n*-Alkanes

n-Alkane	B_1	B_2	B_3	SE[a]
Butane	0.75207×10^{-3}	8.98439	0.026095	0.0050
Pentane	0.28462×10^{-3}	10.38369	0.050929	0.0061
Hexane	0.14643×10^{-3}	11.23805	0.061557	0.0062
Octane	0.3622×10^{-5}	16.53706	0.136257	0.0055

[a] Standard error of estimating η values using the given coefficients. $SE = (\sum [y_i - y_{cal,i}]^2/(n-2))^{1/2}$, where y_i are the experimental values of a given property, $y_{cal,i}$ are the calculated values after regression, and n is the number of data points.

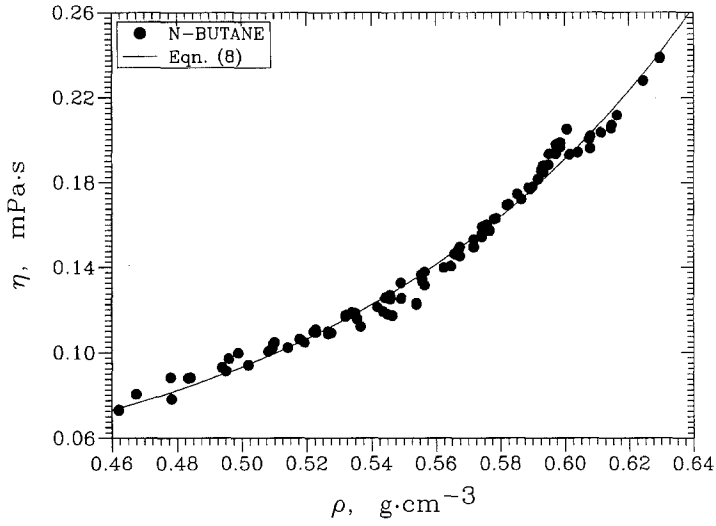

Fig. 5. Variation of the viscosity of *n*-butane as a function of density.

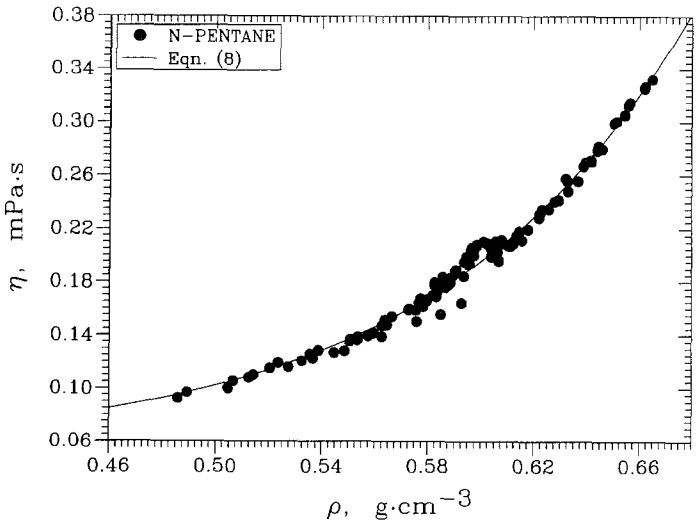

Fig. 6. Variation of the viscosity of *n*-pentane as a function of density.

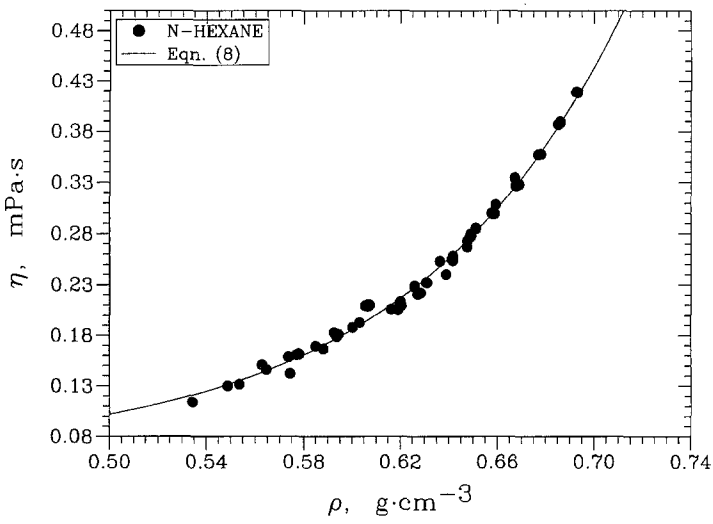

Fig. 7. Variation of the viscosity of *n*-hexane as a function of density.

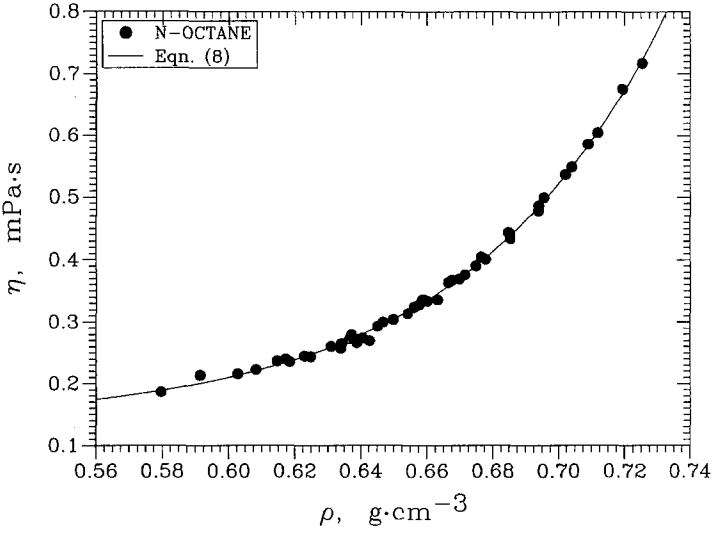

Fig. 8. Variation of the viscosity of *n*-octane as a function of density.

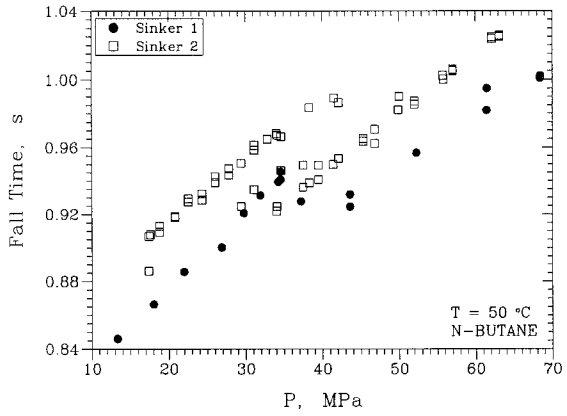

Fig. 9. Variation of the fall time with pressure for sinkers 1 and 2 at 50°C.

also been observed to assume essentially the same values at about 0.205 mPa · s. Although this deviation in viscosity occurs in the same density range for all the alkanes, it corresponds to different combinations of temperatures and pressures when viscosity is plotted as a function of pressure. For each alkane, the pressures around which the anomaly occurs shifts to higher values as the temperature increases. For lower-carbon number alkanes, anomalous region starts to occur at lower temperatures, but still above the boiling point of the corresponding alkane. At pressures

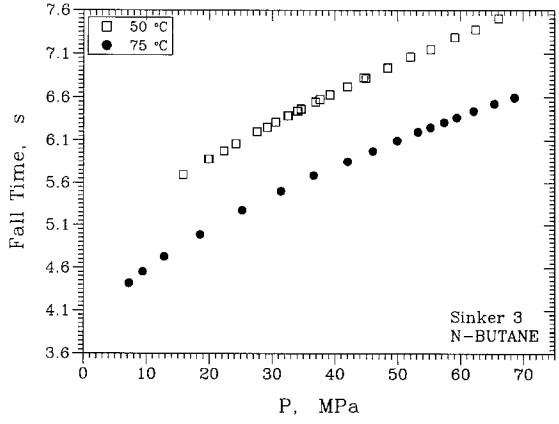

Fig. 10. Variation of the fall time with pressure for sinker 3 at 50 and 75°C.

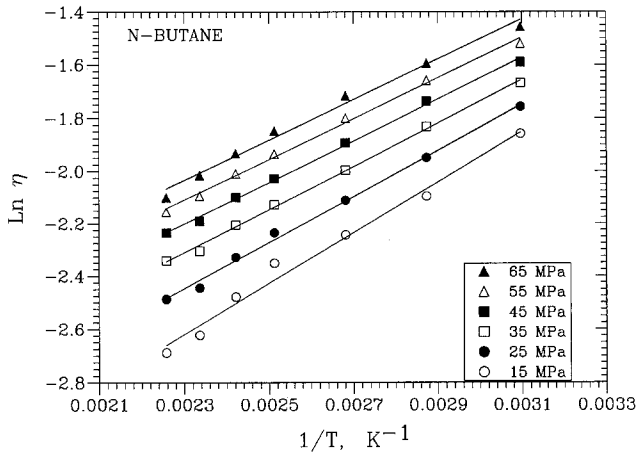

Fig. 11. Variation of the logarithmic viscosity of *n*-butane with the inverse temperature at selected pressures.

and temperatures corresponding to the anomalous behavior, the density, however, varies smoothly with pressure without showing any unusual behavior.

This small localized deviation in viscosity has been investigated in some detail in the present study since a careful examination of viscosity

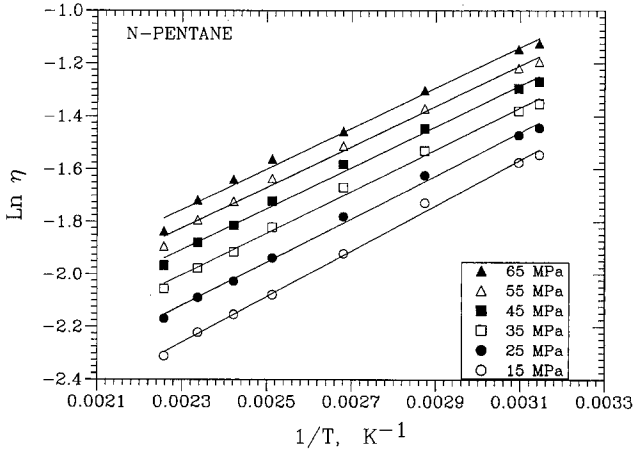

Fig. 12. Variation of the logarithmic viscosity of *n*-pentane with the inverse temperature at selected pressures.

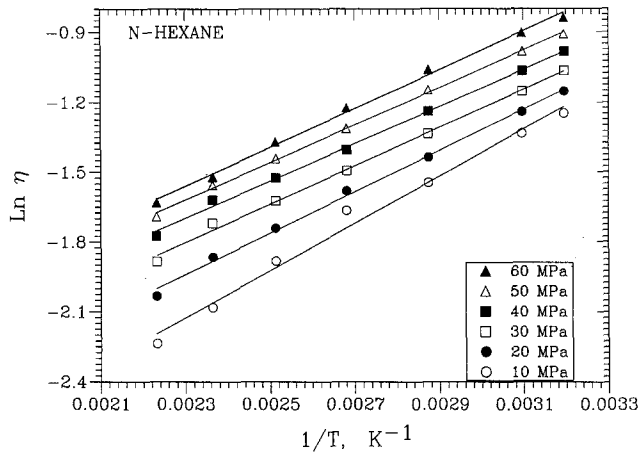

Fig. 13. Variation of the logarithmic viscosity of *n*-hexane with the inverse temperature at selected pressures.

data from the literature [25] showed indications of similar deviations of *n*-butane and *i*-butane. At first, one might consider this to result from scatter in the data. But the viscosity measurements in the present study were repeated several times at the temperatures at which the anomalous deviations were observed. It was found that the anomalous behavior was consistent and regular. Therefore, either this behavior must be attributed to a change in the flow characteristics around the sinker at low viscosities or

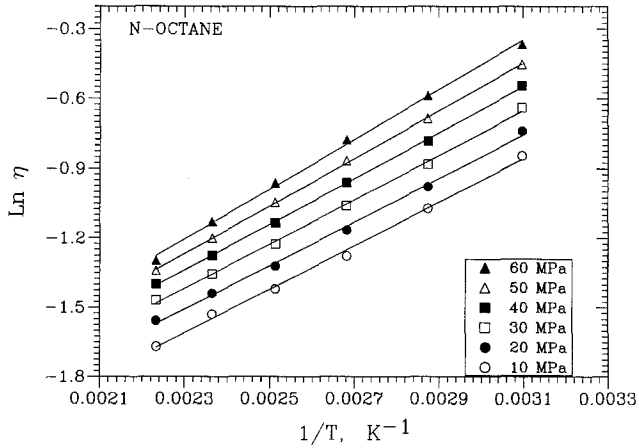

Fig. 14. Variation of the logarithmic viscosity of *n*-octane with the inverse temperature at selected pressures.

it could be interpreted in terms of a "molecule-to-molecular cluster" transition leading to a redistribution of free volume when a specific density is reached with increasing pressure, corresponding to a condition where molecules come within close proximity of each other for the attractive intermolecular forces to become important. As a result of formation of clusters at constant density, even though the total free volume would not

Table IX. Coefficients of the Equation $\ln \eta = A + B/T$ for the Temperature Dependence of Viscosity of *n*-Alkanes at Different Pressures

P (MPa)	A	B	SE[a]
		n-Butane	
15	−4.83601	963.513	1.7×10^{-2}
25	−4.46025	875.188	0.8×10^{-2}
35	−4.19642	819.767	0.6×10^{-2}
45	−4.00710	785.542	0.6×10^{-2}
55	−3.87193	766.340	0.7×10^{-2}
65	−3.77899	758.662	1.2×10^{-2}
		n-Pentane	
15	−4.25425	867.565	0.7×10^{-2}
25	−4.00870	821.899	0.7×10^{-2}
35	−3.82633	792.968	0.8×10^{-2}
45	−3.69029	776.007	0.8×10^{-2}
55	−3.58992	768.077	0.9×10^{-2}
65	−3.51817	767.279	1.1×10^{-2}
		n-Hexane	
10	−4.45538	1012.680	1.9×10^{-2}
20	−3.98045	886.991	0.9×10^{-2}
30	−3.69405	822.282	0.8×10^{-2}
40	−3.53374	797.972	0.7×10^{-2}
50	−3.46665	803.272	0.5×10^{-2}
60	−3.47437	832.187	0.9×10^{-2}
70	−3.54680	881.157	1.8×10^{-2}
		n-Octane	
10	−3.77522	941.719	0.9×10^{-2}
20	−3.67235	941.364	0.8×10^{-2}
30	−3.62034	957.747	0.7×10^{-2}
40	−3.60734	986.707	0.4×10^{-2}
50	−3.62533	1025.440	0.3×10^{-2}
60	−3.66874	1072.000	0.9×10^{-2}
70	−3.73373	1125.090	1.7×10^{-2}

[a] Standard error of estimating $\ln \eta$ values using the given coefficients.

change, the free volume generated between the clusters could be large enough to lead to a viscosity decrease. Upon further increase in pressure, the free volume between clusters would decrease and cause a further increase in viscosity.

For clarification of the phenomenon, further experiments were carried out on the effect of the changes in flow characteristics around the sinker and the measured fall times at viscosities and densities around 0.2 mPa · s and 0.6 g · cm^{-3}, respectively. For this purpose, two additional sinkers of the same overall length and shape, but of densities lower than that used in this study, were constructed by inserting an aluminum core inside the ferromagnetic 416 stainless steel. The sinker-to-fall tube diameter ratios and densities of the sinker used in the present measurements (sinker 1) and the two new sinkers of lower densities (sinker 2 and sinker 3) were 0.9682 and 7.8, 0.9630 and 5.2, and 0.98 and 4.1 g · cm^{-3}, respectively.

Using these sinkers, fall times in *n*-butane were measured and compared at two temperature. The results for sinkers 1 and 2 are shown in Fig. 9. There is some increase in the fall time for sinker 2 over that for sinker 1, but the increase is not large. (The expected increase in the fall time due to a reduction in the density of sinker 2 appears to be offset partly by the somewhat greater gap between this sinker and the fall tube.) As shown in Fig. 9, the flow characteristics for sinkers 1 and 2 are similar, and for both sinkers, in the direction of increasing pressure, the fall times drop suddenly around 35 MPa. This drop around 35 MPa actually represents the local maximum observed in the viscosity-versus-pressure curve of *n*-butane at 323 K. Figure 10 shows the fall times measured using sinker 3. Fall times are significantly increased. More notably, the fall times vary quite smoothly as a function of pressure over the whole pressure range at the two temperatures tested. It is therefore reasonable to assume that the flow characteristics around sinker 3 differ substantially from that around sinker 1. A nonsmooth variation of fall times for sinkers 1 and 2 may be indicative of a transition from laminar to turbulent flow. This is perhaps due to an increased energy loss, when the transition region is entered, delaying the fall of the sinker.

Since the anomaly is localized and its magnitude is relatively small (the largest deviation being less than 7%) (see Figs. 5–8) and since the present calibrations with the NBS certified viscosity standards and high-pressure viscosity data of *n*-hexane cover viscosity ranges below and above the viscosities corresponding to the anomaly, the overall results are not affected. The foregoing analysis is useful in offering a quantitative way to identify the location of transition from laminar to turbulent flow in falling cylinder viscometers. Such analyses may be used as a guide for more accurate viscosity measurements.

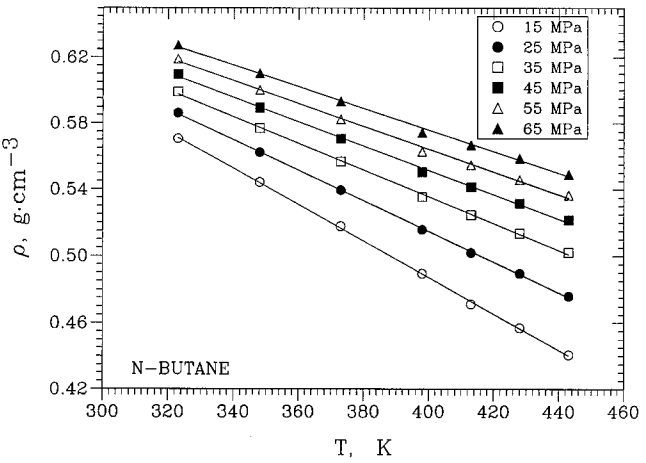

Fig. 15. Variation of the density of *n*-butane with the temperature at selected pressures.

3.3. Effect of Temperature

The temperature dependence of the viscosity and density of these alkanes have also been analyzed. For this purpose, the best polynomial fits were obtained for the data sets given in Tables IV–VII. In obtaining the polynomial fits, the regions of anomaly in the viscosity have been ignored.

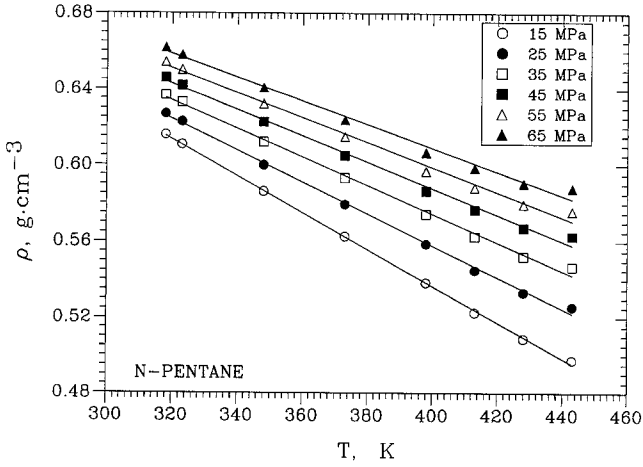

Fig. 16. Variation of the density of *n*-pentane with the temperature at selected pressures.

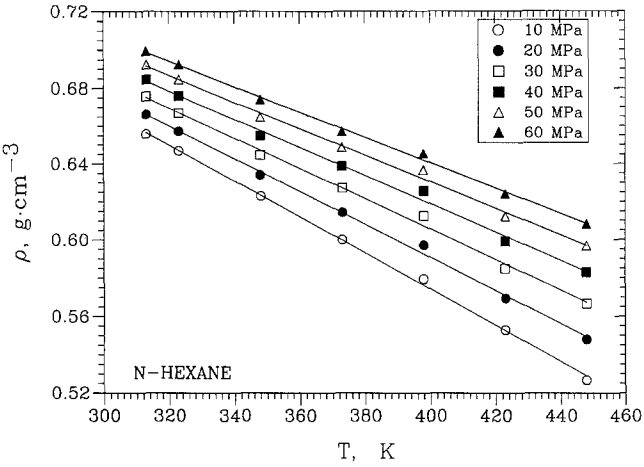

Fig. 17. Variation of the density of *n*-hexane with the temperature at selected pressures.

The coefficients of the polynomials were then used to interpolate the viscosity or density of the alkanes at constant temperatures and pressures.

Figures 11, 12, 13, and 14 show the variation of logarithmic viscosity with inverse temperature for *n*-butane, *n*-pentane, *n*-hexane, and *n*-octane, respectively. The figures show that at a given pressure, the logarithmic

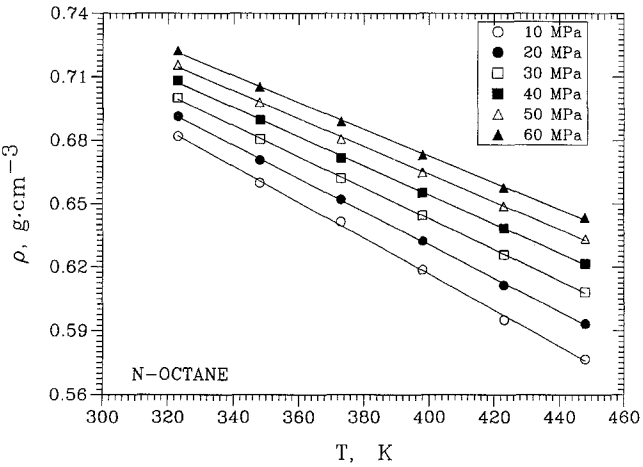

Fig. 18. Variation of the density of *n*-octane with the temperature at selected pressures.

viscosity increases linearly with inverse temperature. The temperature dependence of viscosity can be represented by

$$\ln \eta = A + B/T \tag{9}$$

where η is in mPa · s and T in K as is shown is solid lines in the figures. The coefficients of Eq. (9) are given in Table IX for all alkanes.

Table X. Coefficients of the Linear Equation $\rho = A + BT$ for the Temperature Dependence of Density of *n*-Alkanes at Different Pressures

P (MPa)	A	B	SE[a]
		n-Butane	
15	0.923753	-0.1091×10^{-2}	0.4×10^{-3}
25	0.882537	-0.9195×10^{-3}	0.3×10^{-3}
35	0.857918	-0.8059×10^{-3}	0.5×10^{-3}
45	0.845298	-0.7346×10^{-3}	0.7×10^{-3}
55	0.840077	-0.6894×10^{-3}	0.8×10^{-3}
65	0.837657	-0.6544×10^{-3}	0.7×10^{-3}
		n-Pentane	
15	0.920287	-0.9591×10^{-3}	0.4×10^{-3}
25	0.889340	-0.8288×10^{-3}	0.8×10^{-3}
35	0.871665	-0.7431×10^{-3}	0.1×10^{-2}
45	0.863134	-0.6887×10^{-3}	0.1×10^{-2}
55	0.859619	-0.6523×10^{-3}	0.1×10^{-2}
65	0.857000	-0.6203×10^{-3}	0.1×10^{-2}
		n-Hexane	
10	0.952566	-0.9456×10^{-2}	0.8×10^{-3}
20	0.937517	-0.8667×10^{-3}	0.1×10^{-2}
30	0.925599	-0.7997×10^{-3}	0.1×10^{-2}
40	0.916814	-0.7446×10^{-3}	0.1×10^{-2}
50	0.911161	-0.7013×10^{-3}	0.1×10^{-2}
60	0.908639	-0.6699×10^{-3}	0.8×10^{-3}
70	0.909250	-0.6504×10^{-3}	0.6×10^{-3}
		n-Octane	
10	0.956751	-0.8502×10^{-3}	0.7×10^{-3}
20	0.945346	-0.7872×10^{-3}	0.3×10^{-3}
30	0.936497	-0.7338×10^{-3}	0.3×10^{-3}
40	0.930207	-0.6901×10^{-3}	0.4×10^{-3}
50	0.926474	-0.6560×10^{-3}	0.4×10^{-3}
60	0.925299	-0.6315×10^{-3}	0.5×10^{-3}
70	0.926682	-0.6167×10^{-3}	0.7×10^{-3}

[a] Standard error of estimating ρ values using the given coefficients.

The density data obtained after the interpolations are plotted in Figs. 15, 16, 17, and 18 for *n*-butane, *n*-pentane, *n*-hexane, and *n*-octane, respectively, as a function of temperature. As can be seen, the density decreases linearly with temperature in the temperature range of this study. A linear equation of the form

$$\rho = A + BT \tag{10}$$

where ρ is in $g \cdot cm^{-3}$ and T in K, represents the data well. The coefficients of Eq. (10) are given in Table X for all alkanes.

4. CONCLUSIONS

The viscosity and density of *n*-alkanes increase with the pressure and the carbon number of alkane and decrease with the temperature. The high-pressure viscosity of *n*-butane, *n*-pentane, *n*-hexane, and *n*-octane can be reduced to a single curve when plotted as a function of density. An exponential equation of the form $\eta B_1 \exp(B_2\rho) + B_3$ is shown to describe the density dependence of the alkane viscosities. The logarithmic viscosity of the alkanes shows a linear dependence on the inverse temperature; on the other hand, the density varies linearly with the temperature at all pressures considered in the present study.

REFERENCES

1. K. Stephan and K. Lucas, *Viscosity of Dense Fluids* (Plenum Press, New York, 1979).
2. P. E. Liley, T. Makita, and Y. Tanaka, in *Properties of Inorganic and Organic Fluids*, C. Y. Ho, ed. (Hemisphere, New York, 1988).
3. H. Kashiwagi and T. Makita, *Int. J. Thermophys.* **3**:289 (1982).
4. D. W. Brazier and G. R. Freeman, *Can. J. Chem.* **47**:893 (1969).
5. N. A. Agaev and I. F. Golubev, *Gazov. Promst.* **8**:50 (1963).
6. P. W. Bridgman, *Proc. Am. Acad. Arts Sci.* **61**:57 (1926).
7. J. H. Dymond and K. J. Young, *Int. J. Thermophys.* **1**:331 (1980).
8. J. H. Dymond, J. Robertson, and J. D. Isdale, *Int. J. Thermophys.* **2**:133 (1981).
9. E. Dickinson, *J. Phys. Chem.* **81**:2108 (1977).
10. N. A. Agaev and I. F. Golubev, *Doklady Akademii Nauk SSSR* **151**:597 (1963).
11. Ya. M. Naziev, S. O. Guseinov, and A. K. Akhmedov, *Neft. Gazov. Promst.* **15**:65 (1972).
12. J. H. Dymond, K. J. Young, and J. D. Isdale, *Int. J. Thermophys.* **1**:345 (1980).
13. D. A. Berstad, *Viscosity and Density of n-Hexane, Cyclohexane and Benzene, and Their Binary Mixtures with Methane*, Ph.D. thesis (Universitetet I Trondheim, Norway, 1989).
14. J. H. Dymond and K. J. Young, *J. Chem. Thermodynam.* **11**:887 (1979).
15. R. G. Griskey and L. N. Canjar, *AIChE J.* **5**:29 (1959).
16. D. E. Stewart, B. H. Sage, and W. N. Lacey, *Ind. Eng. Chem.* **46**:2529 (1954).
17. S. E. Babb and G. J. Scott, *J. Chem. Phys.* **40**:3666 (1964).
18. H. H. Reamer, G. Cokelet, and B. H. Sage, *Anal. Chem.* **31**:1422 (1959).

19. A. L. Lee and R. T. Ellington, *J. Chem. Eng. Data* **10**:101 (1965).
20. N. A. Agaev and I. F. Golubev, *Gazov. Promst.* **8**:45 (1963).
21. A. F. Collings and E. McLaughlin, *Trans. Faraday Soc.* **67**:340 (1971).
22. B. H. Sage and W. N. Lacey, *Thermodynamic Properties of the Lighter Paraffin Hydrocarbons and Nitrogen* (American Petroleum Institute, New York, 1950).
23. J. P. Dolan, K. E. Starling, A. L. Lee, B. E. Eakin, and R. T. Ellington, *J. Chem. Eng. Data* **8**:396 (1963).
24. L. T. Carmichael and B. H. Sage, *J. Chem. Eng. Data* **8**:612 (1963).
25. D. E. Diller and L. J. Van Poolen, *Int. J. Thermophys.* **6**:43 (1985).
26. Patent application being processed.
27. J. B. Irwing and A. J. Barlow, *J. Phys. E. Sci. Intr.* **4**:232 (1971).
28. J. B. Irwing, *J. Phys. D Appl. Phys.* **5**:214 (1972).
29. R. J. McLachlan, *J. Phys. E Sci. Inst.* **9**:391 (1976).
30. Y. L. Sen and E. Kiran, *Polym. Preprints* **31**(1):556 (1990).
31. Y. L. Sen and E. Kiran, *J. Supercrit. Fluids* **3**:91 (1990).
32. F. D. Harvey, *Engineering Properties of Steel* (American Society for Metals, Ohio, 1982).
33. R. C. Reid, J. M. Prausnitz, and B. E. Poling, *The Properties of Gases and Liquids*, 4th ed. (McGraw-Hill, New York, 1987).